

## Article

# Fabrication of $\text{Cr}_2\text{AlB}_2$ and $\text{Cr}_4\text{AlB}_4$ MAB Phase Coatings by Magnetron Sputtering and Post-Annealing

 Ke Jia <sup>1</sup>, Guojing Wang <sup>1,2,\*</sup>, Shasha Lv <sup>3</sup>, Yan Li <sup>1,4</sup>, Shengjie Du <sup>3</sup> and Zhengcao Li <sup>1,\*</sup>

<sup>1</sup> State Key Laboratory of New Ceramics and Fine Processing, Key Laboratory of Advanced Materials (MOE), School of Materials Science and Engineering, Tsinghua University, Beijing 100084, China; jiake1441@163.com (K.J.); li-y23@mails.tsinghua.edu.cn (Y.L.)

<sup>2</sup> School of Materials and Energy, Lanzhou University, Lanzhou 730000, China

<sup>3</sup> Key Laboratory of Beam Technology (MOE), College of Nuclear Science and Technology, Beijing Normal University, Beijing 100875, China; lvss@bnu.edu.cn (S.L.); 202121220026@mail.bnu.edu.cn (S.D.)

<sup>4</sup> Department of Engineering Physics, Tsinghua University, Beijing 100084, China

\* Correspondence: wanggj@lzu.edu.cn (G.W.); zcli@tsinghua.edu.cn (Z.L.); Tel.: +86-10-62772233 (Z.L.)

**Abstract:**  $\text{Cr}_2\text{AlB}_2$  and  $\text{Cr}_4\text{AlB}_4$  are members of the MAB phases that exhibit unique properties of both metals and ceramics. However, despite these unique characteristics,  $\text{Cr}_2\text{AlB}_2$  and  $\text{Cr}_4\text{AlB}_4$  phase coatings have not been widely investigated. In this study,  $\text{Cr}_2\text{AlB}_2$  and  $\text{Cr}_4\text{AlB}_4$  MAB phase coatings were fabricated by magnetron sputtering at room temperature and post-annealing. A composite target, consisting of a phase-pure disc-shaped CrB target overlapped by uniformly dispersed fan-shaped Al slices, was placed parallel to the substrates. The Al content of the coatings was adjusted by altering the areal proportion of the Al slices. MAB phases have crystallized upon post-annealing the as-deposited coatings on  $\text{Al}_2\text{O}_3$ (0001) substrates in Ar. The phase compositions and morphologies of the crystalline coatings were found to be dependent on the Al content and the annealing temperature. As-deposited coatings with a Cr:Al:B ratio close to 2:1:2 could crystallize as pure and dense  $\text{Cr}_2\text{AlB}_2$  phases within the temperature range of 650–800 °C; higher annealing temperatures resulted in the decomposition of  $\text{Cr}_2\text{AlB}_2$ , while crystallization at lower temperatures was not evident from X-ray diffraction. As-deposited coatings with a Cr:Al:B ratio close to 3:1:3, despite containing a relatively higher Al content than required by the stoichiometry of  $\text{Cr}_4\text{AlB}_4$ , exhibited insufficient crystallization of  $\text{Cr}_4\text{AlB}_4$  with unknown phases below 840 °C. Higher annealing temperatures resulted in the coexistence of  $\text{Cr}_4\text{AlB}_4$  and CrB, indicating that achieving phase-pure and well-crystallized  $\text{Cr}_4\text{AlB}_4$  coatings proved challenging, possibly due to the inevitable loss of Al during annealing. The configuration of the composite target and the substrates provides a promising strategy for fabricating phase-pure and dense  $\text{Cr}_2\text{AlB}_2$  coatings.

**Keywords:**  $\text{Cr}_2\text{AlB}_2$ ;  $\text{Cr}_4\text{AlB}_4$ ; MAB phases; magnetron sputtering; post-annealing



**Citation:** Jia, K.; Wang, G.; Lv, S.; Li, Y.; Du, S.; Li, Z. Fabrication of  $\text{Cr}_2\text{AlB}_2$  and  $\text{Cr}_4\text{AlB}_4$  MAB Phase Coatings by Magnetron Sputtering and Post-Annealing. *Coatings* **2023**, *13*, 1800. <https://doi.org/10.3390/coatings13101800>

Received: 5 September 2023

Revised: 9 October 2023

Accepted: 17 October 2023

Published: 20 October 2023



**Copyright:** © 2023 by the authors. Licensee MDPI, Basel, Switzerland. This article is an open access article distributed under the terms and conditions of the Creative Commons Attribution (CC BY) license (<https://creativecommons.org/licenses/by/4.0/>).

## 1. Introduction

MAB phases, a group of ternary layered compounds (where M is a transition metal, A is typically Al, and B is boron) [1], are gaining increasing attention due to their resemblance to the well-known MAX phases (with the formula  $\text{M}_{n+1}\text{AX}_n$ , where M is a transition metal, A is a group 13–14 element, X is carbon or nitrogen, and  $n = 1, 2, 3 \dots$ ) [2]. MAX phases and MAB phases feature microstructures characterized by alternating M-X or M-B layers interleaved by A atom layers [3–6]. Unlike the universal formula  $\text{M}_{n+1}\text{AX}_n$  for MAX phases [7], the formula of MAB phases varies depending on different M:B ratios and combinations of M-B slabs and A-layers, including “MAB” (222-type) [5,8], “ $\text{M}_2\text{AB}_2$ ” (212-type) [5,9], “ $\text{M}_3\text{AB}_4$ ” (314-type) [5], “ $\text{M}_4\text{AB}_6$ ” (416-type) [5], and “ $\text{M}_4\text{AB}_4$ ” (414-type) [10]. The inherent characteristic of strong M-B bonds and weak M-A bonds [11] bestows MAB phases with a unique amalgamation of metallic and ceramic properties akin to MAX phases [12], such

as good thermal and electrical conductivities [13,14], high toughness [15], radiation tolerance [16–19], and oxidation resistance [13,20]. These distinctive attributes position MAB phases as promising candidates for applications in high-temperature structural materials.

Within the MAB phase family, the Cr-Al-B system exhibits the greatest structural diversity, featuring four thermodynamically stable Cr-Al-B MAB phases ( $\text{Cr}_2\text{AlB}_2$ ,  $\text{Cr}_4\text{AlB}_4$ ,  $\text{Cr}_3\text{AlB}_4$ , and  $\text{Cr}_4\text{AlB}_6$ ) [5,10]. The synthesis and properties of single crystals, powder, and bulk Cr-Al-B MAB phases have been investigated. Ade et al. synthesized  $\text{Cr}_2\text{AlB}_2$ ,  $\text{Cr}_3\text{AlB}_4$ , and  $\text{Cr}_4\text{AlB}_6$  single crystals through the reaction of Cr, B, and excessive Al powders, with the crystallographic parameters of these crystals determined [5]. Zhang et al. synthesized phase-pure  $\text{Cr}_2\text{AlB}_2$  powders by sintering a mixture of CrB and excessive Al powders, then removing unreacted Al using a NaOH solution [21]. These  $\text{Cr}_2\text{AlB}_2$  powders remained stable up to 900 °C in Ar and partially decomposed into  $\text{Cr}_4\text{AlB}_4$  and/or CrB at elevated temperatures due to the detachment of Al. Additionally, oxidation experiments conducted on  $\text{Cr}_2\text{AlB}_2$  powders in flowing air up to 1200 °C revealed the formation of a protective  $\text{Cr}_2\text{O}_3$  or  $\text{Al}_2\text{O}_3$  scale on grain surfaces, suggesting promising applications for  $\text{Cr}_2\text{AlB}_2$  in high-temperature oxidation-resistant coatings [20]. Kim et al. synthesized bulk  $\text{Cr}_2\text{AlB}_2$ ,  $\text{Cr}_3\text{AlB}_4$ , and  $\text{Cr}_4\text{AlB}_6$  from CrB, B, and Al powders and evaluated the radiation tolerance of these phases in terms of defect kinetics [18]. The newly discovered Cr-Al-B MAB phase,  $\text{Cr}_4\text{AlB}_4$ , was predicted to be thermodynamically stable via first-principle calculations [22] and detected in powders synthesized from a mixture of CrB and Al powders [10]; however, its properties have not yet been investigated experimentally. The formation mechanisms of  $\text{Cr}_2\text{AlB}_2$  and  $\text{Cr}_3\text{AlB}_4$  were studied by Hanner et al. [23], who quenched pellets sintered from mixtures of CrB and Al powders (molar ratios of 2:1.5 and 3:1.5:1 for  $\text{Cr}_2\text{AlB}_2$  and  $\text{Cr}_3\text{AlB}_4$ , respectively) at different temperatures. X-ray diffraction (XRD) tests revealed a topotactic formation process involving the direct intercalation of Al into CrB or  $\text{Cr}_3\text{B}_4$ .

Concerning Cr-Al-B MAB phase coatings, only  $\text{Cr}_2\text{AlB}_2$  coatings have been obtained to date [24].  $\text{Cr}_2\text{AlB}_2$  phases were produced in coatings deposited on MgO(100) substrates that were in situ heated to 680 °C, using a combinatorial magnetron sputtering approach involving three tilt-fixed targets (Cr, Al, and  $\text{AlB}_2$ ). The resulting morphology revealed cuboid or chimney-shaped grains, precluding the formation of dense coatings. In addition, the elemental gradient instigated by the combinatorial method led to the emergence of impurity phases. These limitations necessitate alternative approaches to yield dense and phase-pure  $\text{Cr}_2\text{AlB}_2$  coatings. Encouragement for this endeavor is derived from the successful fabrication of dense MoAlB phase coatings using magnetron sputtering at ambient temperature and subsequent ex situ post-annealing [25], suggesting a promising pathway for achieving dense Cr-Al-B MAB phase coatings through sufficient bulk diffusion of atoms.

Notably,  $\text{Cr}_4\text{AlB}_4$  shares with  $\text{Cr}_2\text{AlB}_2$  the identical theoretical atomic ratio of Cr:B. Given the aforementioned topotactic formation of  $\text{Cr}_2\text{AlB}_2$ , it is reasonable that the fabrication method employed for  $\text{Cr}_2\text{AlB}_2$  coatings may also be applicable to  $\text{Cr}_4\text{AlB}_4$  coatings. In this study, a generic approach for the preparation of both  $\text{Cr}_2\text{AlB}_2$  and  $\text{Cr}_4\text{AlB}_4$  phase coatings has been proposed, involving magnetron sputtering deposition of Cr-Al-B coatings using a composite target composed of CrB and Al, followed by post-annealing at varying temperatures. The morphology and phase composition of the annealed coatings were characterized, and the deposition and post-annealing parameters for achieving dense and phase-pure  $\text{Cr}_2\text{AlB}_2$  phase coatings were elucidated. Furthermore, the effects of the target-substrate configuration on the chemical and phase compositions of the coatings were discussed, which could facilitate improvements in the phase purity of  $\text{Cr}_2\text{AlB}_2$  phase coatings.

## 2. Materials and Methods

$\text{Cr}_2\text{AlB}_2$  and  $\text{Cr}_4\text{AlB}_4$  coatings were fabricated using a two-step method involving deposition by magnetron sputtering at room temperature and subsequent ex situ post-annealing in Ar.

The deposition process was conducted in a surface treatment system equipped with magnetron sputtering modules (FJL-5600, SKY Technology Development Co. Ltd., Shenyang, China, Chinese Academy of Sciences). Considering the identical Cr:B ratio in both  $\text{Cr}_2\text{AlB}_2$  and  $\text{Cr}_4\text{AlB}_4$ , a composite target consisting of a disk-shaped CrB target overlapped by uniformly dispersed fan-shaped Al slices was used as the elemental sources (Figure 1a). In detail, the CrB target, confirmed as phase-pure by X-ray diffraction (XRD), was synthesized through sintering a mixture of Cr and  $\text{CrB}_2$  powders (purity 99.5%, molar ratio 1:1). The as-synthesized CrB bulk was then cut into a disk shape (3 mm in thickness, 60 mm in diameter) and bonded to a Cu backplate (2 mm in thickness, 60 mm in diameter) with silver paste. Al slices with a radius of 30 mm were obtained from a 1 mm thick Al plate (purity 99.999%) by wire cutting. These slices underwent a rigorous process, including polishing with SiC sandpaper, ultrasonic cleaning with acetone, ethanol, and deionized water to remove contaminations, and finally, drying in an oven. The radii of the slices overlapped those of the CrB target, and the total areal proportion of the Al slices in the whole surface area of the underlying CrB disk ranged from 0.20 to 0.31, enabling the adjustment of the relative Al content of the as-deposited coatings. Apart from Cr-Al-B coatings, CrB coatings were also deposited for comparative purposes using a single CrB target with no overlapping Al slices (i.e., the total areal proportion of Al slices was 0). Si(100) and  $\text{Al}_2\text{O}_3(0001)$  single crystal substrates measuring 1 cm  $\times$  1 cm were fixed on the sample holder parallel to the composite target. The substrates were previously subjected to a sequence of ultrasonic cleaning using acetone, ethanol, and deionized water, followed by a drying process. The target-to-substrate distance was 8 cm (Figure 1b). The base pressure in the deposition chamber was below  $2 \times 10^{-4}$  Pa before sputtering. The composite target was sputtered using Ar (purity 99.999%) at 0.3 Pa in the direct current (DC) mode, with the power applied fixed at 60 W during sputtering. The deposition rate was estimated to be 7 nm/min.

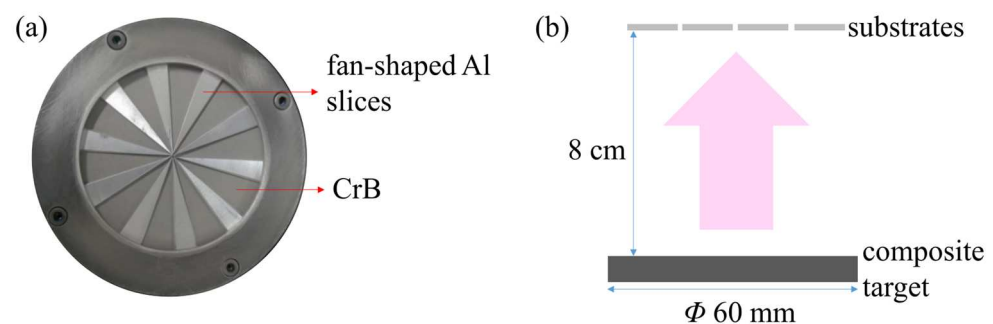


**Figure 1.** The configuration of the target and substrates. (a) Top view of the composite target. Fan-shaped Al slices were dispersed uniformly on the CrB target. (b) Substrates were placed parallel to the composite target.

Each sample (the as-deposited coating on  $\text{Al}_2\text{O}_3(0001)$ ) was transferred to an individual corundum crucible and subjected to post-annealing in a corundum tube furnace in Ar (purity 99.999%). The tube was evacuated to  $5 \times 10^{-2}$  Pa using a vacuum pump and purged with Ar (purity 99.999%) prior to the annealing process. Titanium plates were strategically placed near the crucible to absorb trace amounts of oxygen during annealing. The heating and cooling rates were 5 °C/min. The post-annealed samples were cooled in situ to room temperature for subsequent characterization.

The phase composition of the post-annealed coatings was analyzed using grazing incident X-ray diffraction (GIXRD) on an X-ray diffractometer with  $\text{Cu-K}\alpha$  radiation ( $\lambda = 1.5418 \text{ \AA}$ ) (D8 Advance, Bruker, Karlsruhe, Germany). The incident angle, scanning rate, and step size were 3°, 4°/min, and 0.02°, respectively. Scanning electron microscopy (SEM) (Merlin Compact, Zeiss, Oberkochen, Germany) was employed at an acceleration voltage of 15 kV to investigate the morphology of the post-annealed coatings. The sample for the transmission electron microscopy (TEM) analysis was prepared by focused ion beam (FIB) conducted on a Helios G4 PFIB CXe DualBeam FIB/SEM (Thermo Fisher, Waltham,

MA, USA) with an Xe ion source. The sample was thinned to c.a. 60 nm for electron transparency. High-resolution TEM (HRTEM) images were obtained using a JEM-2100Plus microscope (JEOL, Tokyo, Japan) at an acceleration voltage of 200 kV.

The authors found that as-deposited coatings on Si(100) underwent a reaction with Si and formed Cr-Al-Si phases when subjected to high-temperature post-annealing, in analogy with the findings reported in [24]. Consequently, these coatings were not subjected to further post-annealing and remained as is for measuring the atomic ratio of the Cr, Al, and B elements using inductively coupled plasma optical emission spectrometry (ICP-OES) (iCAP 6300, Thermo Fisher, Waltham, MA, USA). The ICP-OES results exhibited relative standard deviations of less than 2%. It should be noted that coatings on Al<sub>2</sub>O<sub>3</sub>(0001) substrates were deemed unsuitable for such measurements due to potential interference from Al present in Al<sub>2</sub>O<sub>3</sub>(0001).

In this study, the areal proportion of Al slices in the composite target ranged from 0 to 0.31, achieved by setting the total central angle of the fan-shaped slices as 0°, 72°, 80°, 90°, or 110°. For clarity, abbreviated strings (Table 1) are used in the following text to distinguish coatings based on the substrates, the total central angle of the Al slices, and the post-annealing conditions (for coatings deposited on Al<sub>2</sub>O<sub>3</sub>(0001) substrates). For example, “S72” represents as-deposited coatings on Si(100) derived from a composite target with a total central angle of 72° for the Al slices; “A90p800/9” represents coatings initially deposited on Al<sub>2</sub>O<sub>3</sub>(0001) from a composite target with a total central angle of 90° for the Al slices and post-annealed at 800 °C for 9 h. The long holding time and high holding temperature were selected to ensure complete crystallization of the coatings. Notably, since the coating and substrate are inseparable, these strings may also refer to both the coating and the corresponding substrate, representing the entire sample.

**Table 1.** Abbreviations for the coatings.

Abbreviated Strings	Descriptions	Examples
S[number]	As-deposited coatings on Si(100): S = Si(100) substrate; [number] = the total central angle value of the Al slices (unit: °).	S72 S90
A[number]	As-deposited coatings on Al <sub>2</sub> O <sub>3</sub> (0001): A = Al <sub>2</sub> O <sub>3</sub> (0001) substrate; [number] = the total central angle value of the Al slices (unit: °).	A90
A[number]p	Post-annealed coatings initially deposited on Al <sub>2</sub> O <sub>3</sub> (0001): A = Al <sub>2</sub> O <sub>3</sub> (0001) substrate; [number] = the total central angle value of the Al slices (unit: °).	A80p
A[number]p[T]/[t] *	Post-annealed coatings initially deposited on Al <sub>2</sub> O <sub>3</sub> (0001): A = Al <sub>2</sub> O <sub>3</sub> (0001) substrate; [number] = the total central angle value of the Al slices (unit: °); [T] = the isothermal holding temperature during annealing (unit: °C); [t] = the isothermal holding time during annealing (unit: h).	A0p700/8 A90p800/9 A110p800

\* [t] is omitted if not explicitly indicated.

### 3. Results and Discussion

#### 3.1. Coatings with Varying Al Contents

In the initial attempt, A72, A80, A90, and A110 coatings were subjected to tentative post-annealing processes at 800 °C and 900 °C to investigate their phase compositions. Figure 2 shows the GIXRD patterns of these coatings after post-annealing at 800 °C for 9 h (Figure 2a) and at 900 °C for 7 h (Figure 2b). PDF cards #72-1847 and #32-0277 were used to identify Cr<sub>2</sub>AlB<sub>2</sub> and CrB phases, respectively. Cr<sub>4</sub>AlB<sub>4</sub> was identified using the data reported in [10]. As depicted in Figure 2a, the increase in the Al content resulted in improved crystallinity. A80p800 and A90p800 coatings crystallized as the Cr<sub>2</sub>AlB<sub>2</sub> phase. The XRD peaks of A90p800 were sharper and more distinct than those of A80p800, indicating better crystallinity for A90p800 and a slight sub-stoichiometric Al content in A80p800. A110p800, with an excessive Al content, showed (0k0) preferred orientations. As

the Al content decreased (A72p800), the XRD peaks did not perfectly match those of either  $\text{Cr}_2\text{AlB}_2$  or  $\text{Cr}_4\text{AlB}_4$ , indicating a possible intermediate state between  $\text{Cr}_2\text{AlB}_2$  and  $\text{Cr}_4\text{AlB}_4$ . A higher post-annealing temperature (900 °C) shifted the phase towards Al-depletion (Figure 2b). A72p900 crystallized as  $\text{Cr}_4\text{AlB}_4$  and CrB. A80p900 and A90p900 exhibited three coexisting phases:  $\text{Cr}_2\text{AlB}_2$ ,  $\text{Cr}_4\text{AlB}_4$ , and CrB. In contrast to A110p800, excessive Al was not detected in A110p900, whereas the preferred orientation remained.

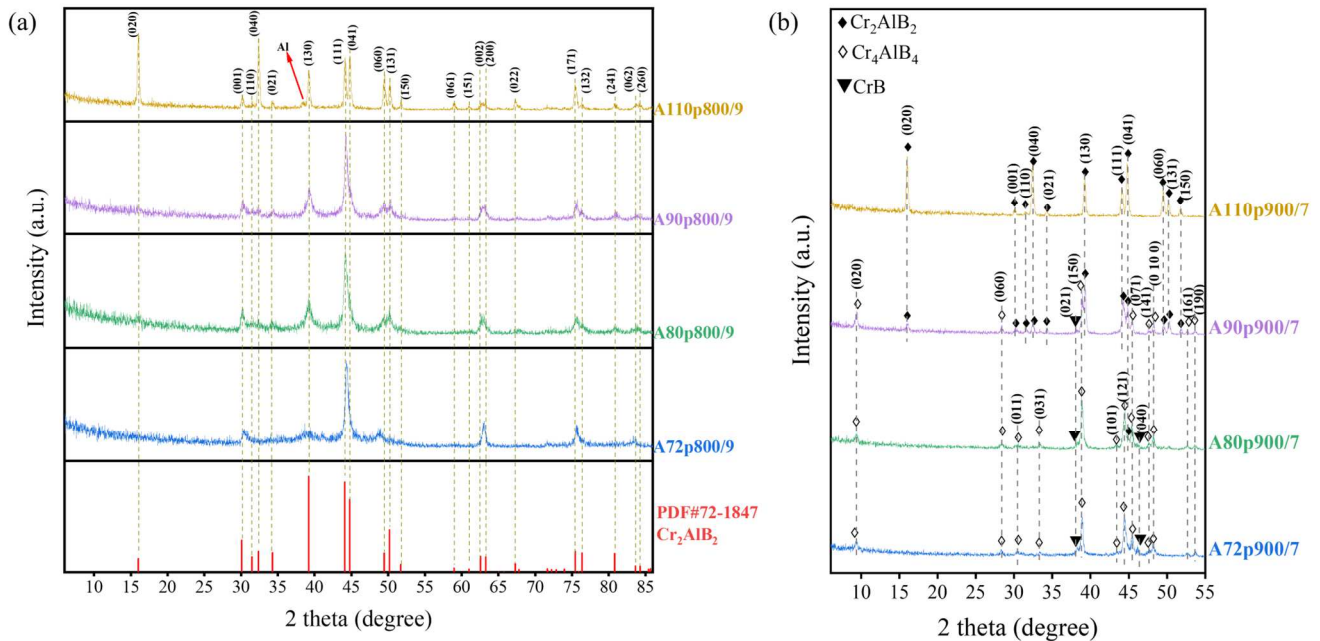


**Figure 2.** GIXRD patterns of the post-annealed coatings on  $\text{Al}_2\text{O}_3(0001)$ . (a) 800 °C for 9 h; (b) 900 °C for 7 h.

The phases identified in Figure 2 are summarized in Figure 3a. The chemical compositions of the as-deposited coatings are also provided in Figure 3b for clarity. Figure 3 underscores that the phase compositions of the coatings depend on the Al content and the post-annealing temperatures.

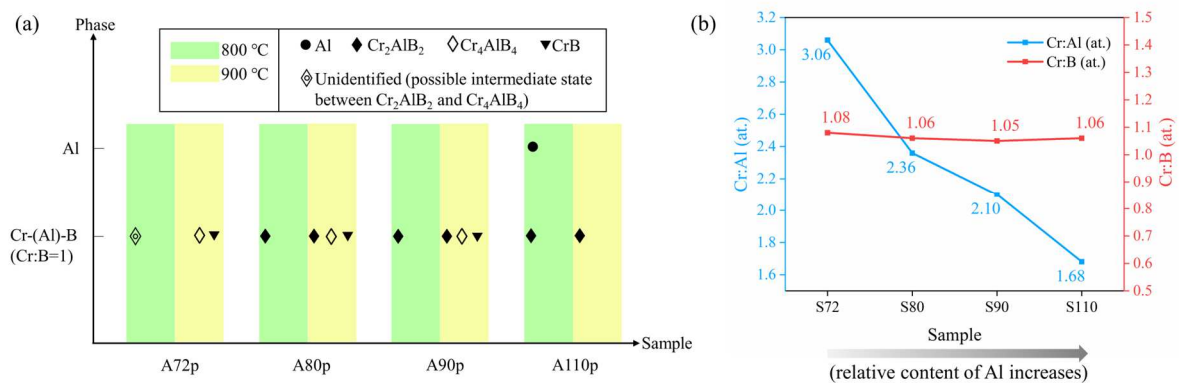


**Figure 3.** (a) A summary of the phases identified in the post-annealed coatings. (b) The chemical compositions (atomic ratio) of the as-deposited coatings.

- The effect of the post-annealing temperature

In general, a higher post-annealing temperature promotes the conversion of Al-rich phases into Al-depleted counterparts. In the case of S72, the Cr:Al:B ratio closely approximated 3:1:3, aligning with the phase status of A72p800. However, the coexistence of  $\text{Cr}_4\text{AlB}_4$  and CrB phases in A72p900 indicates a Cr:Al ratio exceeding 4, signifying a

significant loss of Al. For both A80p and A90p, the  $\text{Cr}_2\text{AlB}_2$  phase detected in samples annealed at 800 °C decomposed into  $\text{Cr}_4\text{AlB}_4$  and CrB at an elevated temperature (i.e., 900 °C), which conformed to the decomposition mechanism of  $\text{Cr}_2\text{AlB}_2$  powders [20]. In the case of A110p, the disappearance of the excessive Al in A110p900 also suggests a loss of Al. The loss of Al from the matrix could be attributed to the outward diffusion of Al at high temperatures [20,26]. Zhang et al. reported that  $\text{Cr}_2\text{AlB}_2$  powders annealed in Ar at temperatures exceeding 900 °C decompose into Al-depleted phases, with the lost Al either evaporating or being oxidized to  $\text{Al}_2\text{O}_3$  [20]. Tang et al. found a reduction in the Al content of Ti-Al-C coatings annealed at 800 °C, attributing it to the diffusion of Al towards the surface and subsequent oxidation [26]. In our experiments, the residual oxygen in the deposition chamber and the adsorbed oxygen during the transfer of samples could lead to the oxidation of Al during annealing, but XRD results showed no apparent peaks of oxides. In addition, grey zones near the samples were observed on the corundum crucible surface, and the grey zones near the samples annealed at 900 °C were conductive. These factors imply the evaporation of Al during annealing, and the potential oxidation of Al is deemed negligible. Given that Al-containing MAB phases have been obtained after long-time annealing, the loss of Al was very likely to occur concurrently with the crystallization of the coatings and then ceased upon completion of the crystallization.

- The effect of the Al content

The Cr:B ratios of all four coatings closely approximated 1 (Figure 3b), indicating that the Cr:B ratio in the CrB target remains consistent in the coatings and is unlikely to be influenced by the Al content. However, the effect of the Al content becomes evident through the phase compositions of the annealed coatings. Phase-pure  $\text{Cr}_2\text{AlB}_2$  could be formed at 800 °C when the Al content satisfied the stoichiometric requirement. Al-depletion (S72 in Figure 3b) failed to yield  $\text{Cr}_2\text{AlB}_2$ , while a slight sub-stoichiometry of Al (S80 and S90 in Figure 3b) did not impede the formation of  $\text{Cr}_2\text{AlB}_2$ . As the Al content exceeded the stoichiometric proportions (S110 in Figure 3b),  $\text{Cr}_2\text{AlB}_2$  coexisted with Al. It should be highlighted that excessive Al is unnecessary for the formation of  $\text{Cr}_2\text{AlB}_2$  coatings in this study. In contrast, the synthesis of single crystal, bulk, and powder  $\text{Cr}_2\text{AlB}_2$  from powder reactants necessitates excessive Al [5,18,21]. This divergence could be ascribed to the degree of mixing the Cr, Al, and B elements. Coatings deposited through magnetron sputtering exhibit homogenous atomic-level mixing of Cr, Al, and B elements. In contrast, the synthesis of single crystals, bulk, and powder  $\text{Cr}_2\text{AlB}_2$  entails long-range interdiffusion of elements due to the grain size of the powder reactants (often in the order of micrometers). For all coatings annealed at 900 °C, the increase in Al content corresponded to a decrease in the Cr:Al ratios of the phases, indicating that the unevaporated Al satisfied the stoichiometric requirements of the thermodynamically stable phases [20].

SEM images of the coatings are presented in Figure 4. In the case of A110p800, the excessive Al in A110 facilitated the growth of stick-shaped  $\text{Cr}_2\text{AlB}_2$  grains infiltrated by molten Al at high temperatures (as indicated by the liquid-like zone enclosed in the red dashed line in Figure 4m). The molten Al may have served as reservoirs for the nucleation of  $\text{Cr}_2\text{AlB}_2$  nuclei and as a rich source of Al for the expansion of the grains. As for A80p800 and A90p800, the amount of Al could only satisfy the local growth of  $\text{Cr}_2\text{AlB}_2$  nuclei, and the growth process terminated before the grains could expand extensively, thus resulting in densely packed small grains in the coatings (Figure 4e,f,i,j). Regarding A72, the lower Al content was insufficient for the nucleation of  $\text{Cr}_2\text{AlB}_2$ , resulting in unknown Cr-Al-B phases (Figure 4a,b). At the elevated temperature of 900 °C, excessive Al in A110 compensated for the loss of Al, and the pure  $\text{Cr}_2\text{AlB}_2$  phase remained (Figure 3a). However, other coatings crystallized as mixed phases (Figure 3a), exhibiting an uneven surface and protruding grains, which may be attributed to the rapid growth of Cr-(Al)-B grains along specific crystallographic directions.

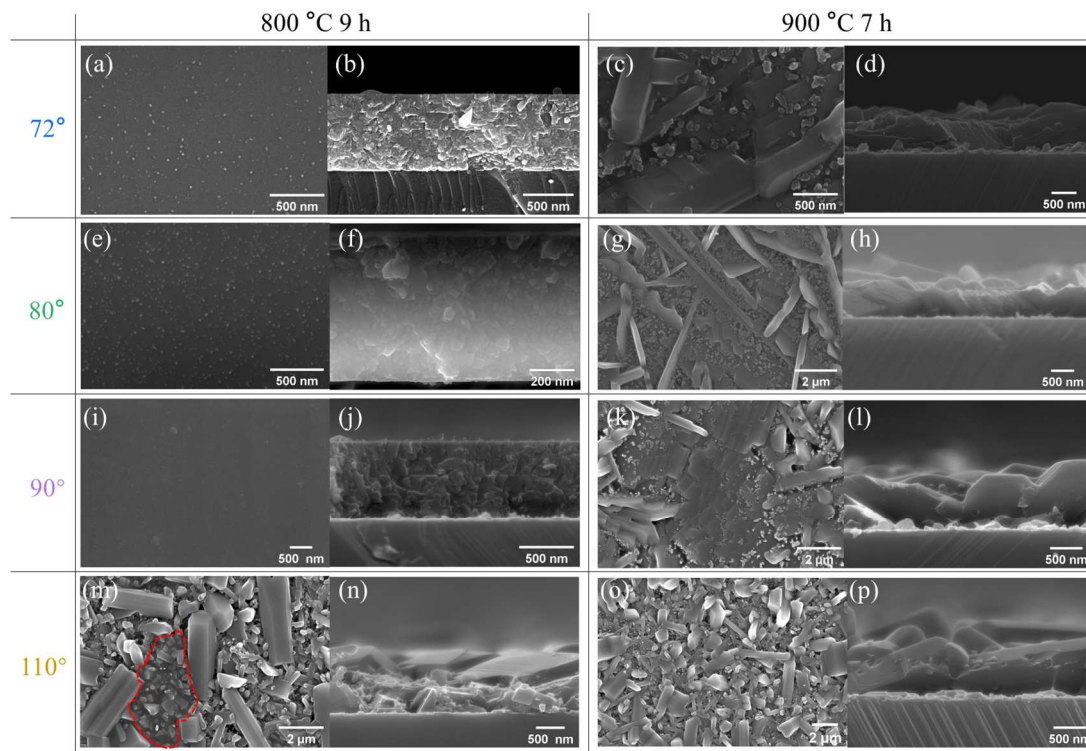


**Figure 4.** SEM images of the coatings. In each combination of Al content and post-annealing parameters, the image on the left (a,c,e,g,i,k,m,o) is the top view of the coating, and the image on the right (b,d,f,h,j,l,n,p) is the cross-section view of the coating.

The comprehensive investigations above have allowed us to identify advantageous parameters for obtaining phase-pure  $\text{Cr}_4\text{AlB}_4$  and  $\text{Cr}_2\text{AlB}_2$  coatings. With A90 meeting the Al content requirement for pure  $\text{Cr}_2\text{AlB}_2$ , further studies regarding the annealing conditions could be carried out to broaden the range of preparation conditions (see Section 3.2). While A72 already possesses an Al content beyond that required for  $\text{Cr}_4\text{AlB}_4$ , the appearance of the CrB phase at 900 °C necessitates further adjustment to the annealing temperature to avoid the appearance of CrB, thus realizing the preparation of phase-pure  $\text{Cr}_4\text{AlB}_4$  (see Section 3.3).

### 3.2. $\text{Cr}_2\text{AlB}_2$ Coatings from A90

The crystallization behavior of  $\text{Cr}_2\text{AlB}_2$  coatings was further studied by annealing A90 coatings at temperatures between 500 °C and 850 °C. Figure 5a shows the GIXRD patterns of the coatings. Coatings annealed below 600 °C, including the as-deposited coatings, remained X-ray amorphous. At 600 °C, XRD peaks of  $\text{Cr}_2\text{AlB}_2$  emerged with poor crystallinity. Peaks became sharper above 635 °C, indicating the overall crystallization of the coatings. At the temperature range of 650–800 °C, the as-deposited coatings crystallized as phase-pure  $\text{Cr}_2\text{AlB}_2$ , and the increase in temperature resulted in improved crystallinity reflected by the peak widths. However, temperatures exceeding 800 °C led to the decomposition of  $\text{Cr}_2\text{AlB}_2$  [20]. As mentioned previously, the formation mechanism of bulk  $\text{Cr}_2\text{AlB}_2$  involves the topotactic reaction between CrB particles and liquid Al [23]. CrB and liquid Al coexist at 680 °C (above the melting point of Al) and directly react to form  $\text{Cr}_2\text{AlB}_2$  at higher temperatures. In our study, no phases such as Al, CrB, or  $\text{Cr}_4\text{AlB}_4$  were identified before  $\text{Cr}_2\text{AlB}_2$  was detected, which implies that the growth of CrB grains did not occur. It could be inferred that the as-deposited coatings underwent the nucleation of CrB and the prompt intercalation of Al atoms into the adjacent CrB skeletons. The relatively lower crystallization temperature here (not exceeding 650 °C) may be attributed to the thorough atomic-level mixing of Cr, Al, and B atoms during sputtering, which avoids the

long-range diffusion of Al atoms in CrB particles in the case of [23]. Furthermore, it is reasonable that the Cr-B bonding in the target may have been partially preserved in the as-deposited coatings, which facilitated the formation of the CrB skeletons. In order to illustrate the role of Al in the formation of  $\text{Cr}_2\text{AlB}_2$ , as-deposited CrB coatings (A0) were post-annealed at the temperature range of 550–750 °C for 8 h. Remarkable crystallization of the CrB phase with discrete and sharp XRD peaks required an annealing temperature as high as 750 °C (Figure 5b). Considering the solvent effect of liquid Al [27], it could be proposed that Al lowers the nucleation temperature of CrB in A90 and reacts with CrB nuclei to form  $\text{Cr}_2\text{AlB}_2$ .

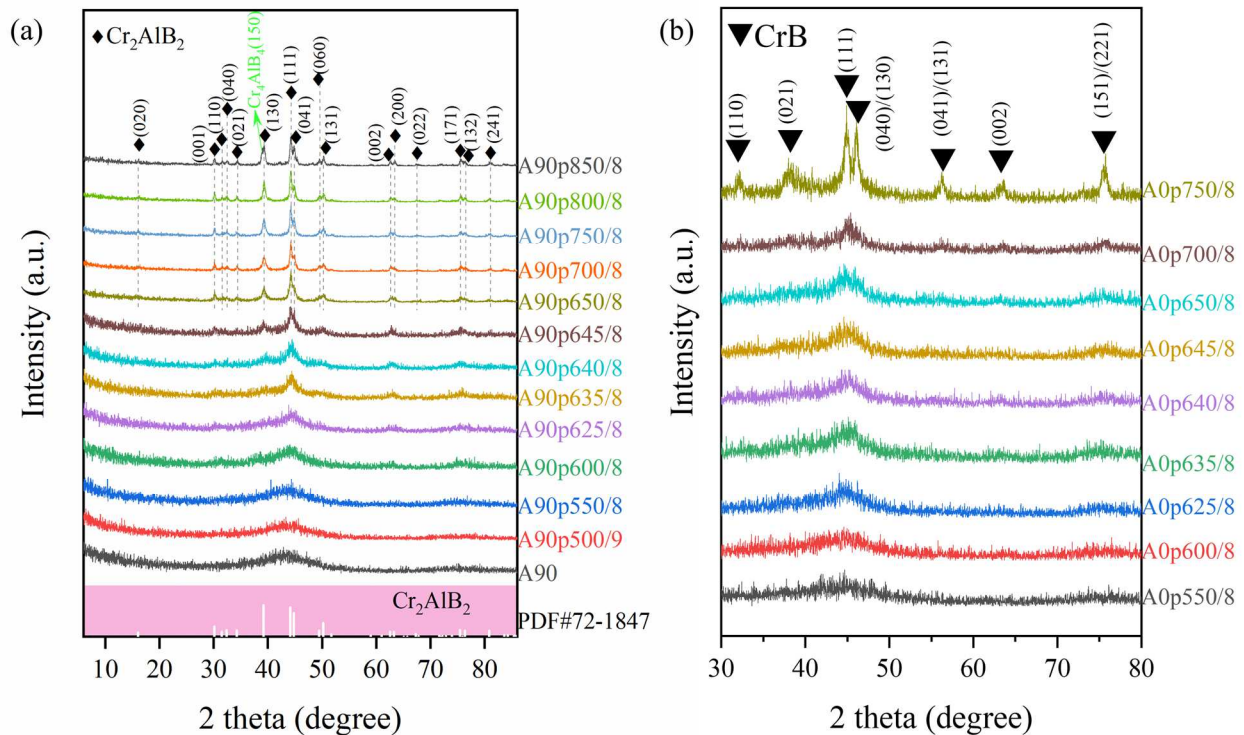
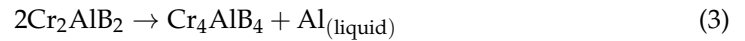
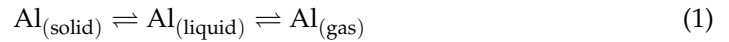


**Figure 5.** (a) GIXRD patterns of A90 and A90p coatings post-annealed at variant temperatures. The reflection peaks of  $\text{Cr}_2\text{AlB}_2$  are indexed in black. (b) GIXRD patterns of CrB (A0) coatings post-annealed at variant temperatures.

Grey zones were also observed on the corundum crucible surface near the A90p samples annealed at 600–850 °C, and the zone near the A90p850 sample was conductive. The lowest temperature required for observing the grey zones (600 °C) coincided with that required for the emergence of  $\text{Cr}_2\text{AlB}_2$  phases (A90p600 in Figure 5a). In contrast, such grey zones were not observed near the annealed CrB coatings. These phenomena further suggest that the loss of Al occurred as a competitive process to the crystallization of the coatings. Thus, the formation and decomposition mechanisms of  $\text{Cr}_2\text{AlB}_2$  coatings could be summarized as follows:

- (i) At temperatures below 600 °C, the crystallization cannot be activated due to insufficient temperatures.
- (ii) As the temperature approaches the melting point of Al (660 °C), enhanced mobility of Al facilitates the nucleation of CrB skeletons and the intercalation of Al. Simultaneously, the loss of Al occurs due to the outward diffusion of Al to the surface and the subsequent evaporation as a competitive process to the crystallization of  $\text{Cr}_2\text{AlB}_2$  (Equations (1) and (2)). Above 650 °C, the  $\text{Cr}_2\text{AlB}_2$  phase crystallizes completely.
- (iii) At temperatures exceeding 800 °C, the  $\text{Cr}_2\text{AlB}_2$  phase tends to decompose into Al (lost) and  $\text{Cr}_4\text{AlB}_4$  (Equations (3) and (4)).



The temperature appears to exert a more significant influence than the duration of the annealing process. GIXRD patterns of A90p650/8, A90p800/2, and A90p800/9 coatings (Figure 6) exhibit a well-crystallized  $\text{Cr}_2\text{AlB}_2$  phase, in line with the SEM images in Figure 7. The grain size of the coatings increased from 650 °C to 800 °C. In comparison, coatings annealed at 800 °C for 2 h or 9 h possessed identical grain sizes, indicating that the grain growth was complete at the early stage of the isothermal holding period. Figure 7g shows the HRTEM image of A90p800/9. The characteristic nanolaminated structure of the MAB phase could be observed. The interplanar spacings,  $d$ , of (020) planes (0.574 nm) and (111) planes (0.208 nm) were noted, aligned with the PDF card #72-1847 values (where  $d_{020} = 0.5535$  nm and  $d_{111} = 0.2052$  nm).

To summarize, the optimal conditions for obtaining dense and phase-pure  $\text{Cr}_2\text{AlB}_2$  coatings have been identified. As-deposited coatings with a Cr:Al:B ratio close to stoichiometry (2:1:2) are recommended for post-annealing at a selected temperature range of 650–800 °C. These conditions result in the formation of dense, phase-pure, and well-crystallized  $\text{Cr}_2\text{AlB}_2$  coatings. A broader range of post-annealing temperatures provides diverse options for the large-scale preparation of  $\text{Cr}_2\text{AlB}_2$  coatings.

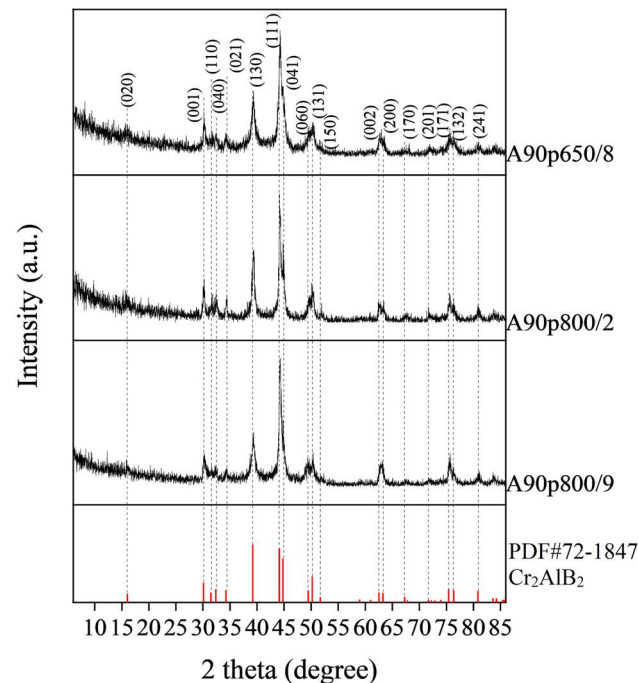
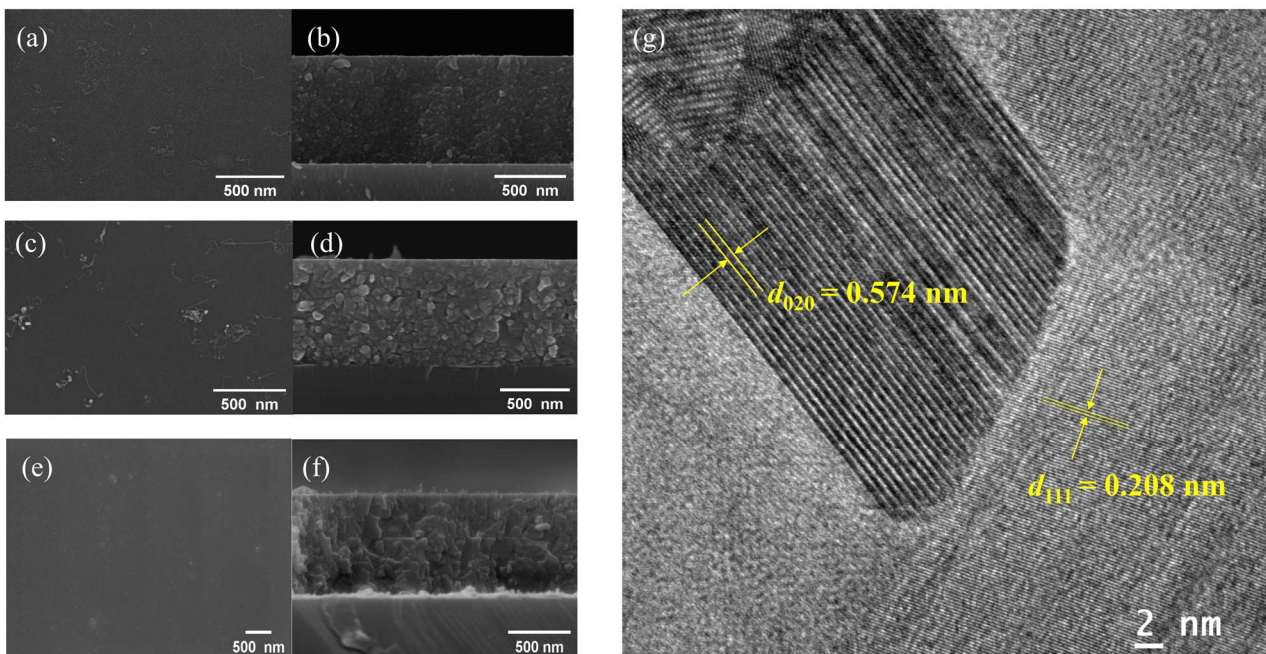


Figure 6. GIXRD patterns of A90p650/8, A90p800/2, and A90p800/9.



**Figure 7.** SEM and TEM images of A90p. (a,b) SEM top view and cross-section of A90p650/8. (c,d) SEM top view and cross-section of A90p800/2. (e,f) SEM top view and cross-section of A90p800/9. (g) HRTEM bright-field image of A90p800/9.

### 3.3. $\text{Cr}_4\text{AlB}_4$ Coatings from A72

The chemical composition of S72 and the phase composition of A72p (Figure 3) demonstrated that the Cr:Al ratio increased from approximately 3 at room temperature to greater than 4 at 900 °C due to the loss of Al. This deduction enlightened us to lower the annealing temperature with the expectation of yielding phase-pure  $\text{Cr}_4\text{AlB}_4$  coatings. Figure 8a shows the GIXRD patterns of A72 post-annealed at 700–850 °C. The A72p700 pattern showed a broad hump, indicating poor crystallinity. As the temperature increased, non-MAB phases (e.g., CrB or Al) were not detected, whereas the (011) peak of  $\text{Cr}_4\text{AlB}_4$  could be directly detected, suggesting a direct transformation from the Cr-Al-B amorphous phase to crystalline  $\text{Cr}_4\text{AlB}_4$ . The broad humps enclosed in the grey rectangles were difficult to identify due to poor crystallinity. At 800 °C and 840 °C, the  $\text{Cr}_4\text{AlB}_4$ (121) peak could be identified, but the highest peaks at other temperatures fell between the  $2\theta$  values of the  $\text{Cr}_2\text{AlB}_2$ (111) peak and the  $\text{Cr}_4\text{AlB}_4$ (121) peak. In other words, well-crystallized  $\text{Cr}_4\text{AlB}_4$  could not be obtained. As the temperature increased to 840 °C, CrB became detectable, indicating the Cr:Al ratios exceeding 4. From a compositional perspective, the decrease in the Al content could be ascribed to the enhanced loss of Al during annealing at elevated temperatures. Lower temperatures (lower than 840 °C) thus seem promising for obtaining pure  $\text{Cr}_4\text{AlB}_4$  (i.e., Cr:Al = 4), but the unidentified peaks fail to support this hypothesis.

A mechanism to explain the coexistence of sharp and broad peaks could be proposed as follows. The relatively lower Al content in A72 cannot meet the requirements for forming  $\text{Cr}_2\text{AlB}_2$ , as demonstrated in A90p (see Section 3.2). Al atoms are enriched in the vicinity of existing CrB nuclei to enhance their local growth and the subsequent intercalation of Al to form  $\text{Cr}_4\text{AlB}_4$  grains. The enrichment leaves behind Al-depleted zones between  $\text{Cr}_4\text{AlB}_4$  grains. Any unreacted Al (if present) will either evaporate or remain within the Al-depleted zones, which is insufficient for forming new  $\text{Cr}_4\text{AlB}_4$  grains. Ungrown Cr-Al-B nuclei thus result in poor crystallinity with XRD humps. Inhomogeneous grain sizes serve as evidence for this explanation (Figure 8b,c). As the temperature exceeds 835 °C, the more substantial loss of Al results in the appearance of the CrB phase.

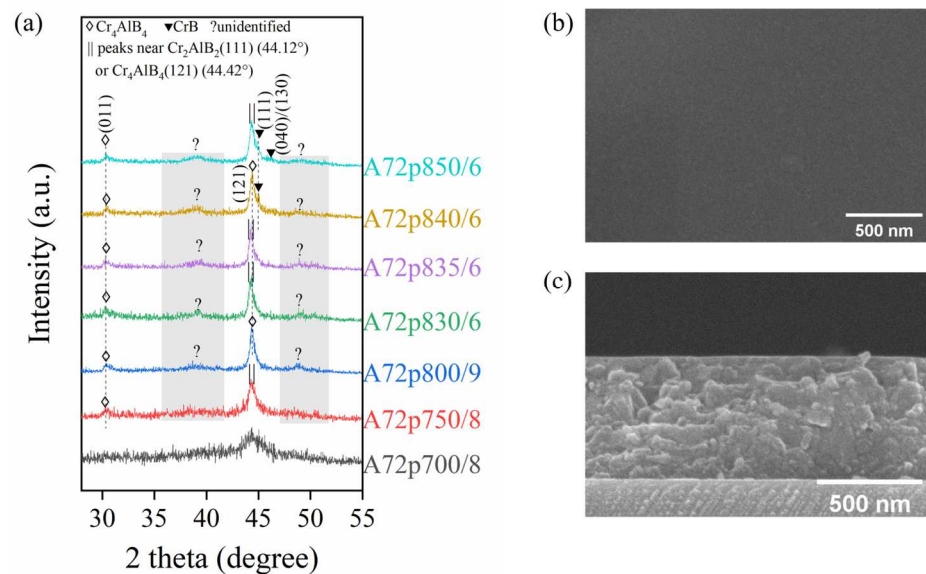


**Figure 8.** A72 coatings annealed at 700–850 °C. (a) GIXRD patterns. (b) Top view of A72p835/6. (c) Cross-section view of A72p835/6.

In summary, phase-pure and well-crystallized  $\text{Cr}_4\text{AlB}_4$  coatings cannot be obtained within our current methods despite previous DFT calculations [22] predicting the stability of  $\text{Cr}_4\text{AlB}_4$ . Further investigations on mitigating the loss of Al are expected to facilitate the formation of phase-pure  $\text{Cr}_4\text{AlB}_4$  coatings.

### 3.4. Supplementary Discussion on the Configuration of Targets and Substrates

All the aforementioned coatings were deposited using a composite target. The configuration of Al slices overlapping the CrB target can be seen as a variation of the combinatorial approach. However, the general combinatorial sputtering of tilt-fixed multi-targets tends to cause the inhomogeneous distribution of elements in the MAB phase coatings [24,28]. Impurities such as  $\text{Cr}_3\text{AlB}_4$  and  $\text{CrB}_2$  were found in an attempt to prepare  $\text{Cr}_2\text{AlB}_2$  coatings by sputtering tilt-fixed Cr, Al, and  $\text{AlB}_2$  targets [24]. Another MAB phase coating,  $\text{MoAlB}$ , was generated by combinatorial magnetron sputtering of tilt-fixed MoB and Al targets and crystallized in situ at 700 °C as  $\text{MoAlB}$ ,  $\text{AlB}_2$ , and Mo-B binary phases. This indicated a deviation from the Mo:B ratio of 1:1 [28]. In our research,  $\text{Cr}_2\text{AlB}_2$  coatings were also prepared by combinatorial sputtering of tilt-fixed CrB and Al targets, followed by ex situ post-annealing for comparison. Three sites (a, b, and c) along the radius of the circular sample plate were selected to position substrates. Detailed parameters are available in Figure S1 in the Supplementary Material. The chemical compositions of the as-deposited coatings on Si(100) were measured by ICP-OES (Table 2). All coatings contained excessive amounts of Al, and the Cr:B ratio ranged from 1.15 to 1.19. The deviation from the theoretical Cr:Al:B ratio (2:1:2) resulted in the coexistence of  $\text{Cr}_2\text{AlB}_2$  and Cr-Al binary phases in the post-annealed coatings on  $\text{Al}_2\text{O}_3(0001)$  (Figure S2).

**Table 2.** The chemical composition of the as-deposited coatings by combinatorial sputtering.

Sample Site	Cr:Al (at.)	Cr:B (at.)
(a) (near the periphery)	0.881	1.15
(b) (in the middle)	0.869	1.19
(c) (near the center)	0.846	1.19

It is noteworthy that our method of sputtering the composite target and the parallel configuration of target-substrates effectively addressed the issue that the atomic ratio of Cr:B in the coatings deposited using the aforementioned combinatorial approach deviated

from 1:1. The precise control of Cr:B ratio, as well as the relative Al content, guarantees the phase purity of the  $\text{Cr}_2\text{AlB}_2$  coatings, which is the core advantage of our method. Moreover, this approach requires only one magnetron site, simplifying the equipment requirements for coatings. It is reasonable to deduce that the composite configuration is not limited to Al slices overlapping the underlying CrB target. Alternately arranged CrB blocks and Al blocks may also be viable, provided the Cr:B ratio is closely controlled around 1.

#### 4. Conclusions

In this study, a two-step method of fabricating  $\text{Cr}_2\text{AlB}_2$  and  $\text{Cr}_4\text{AlB}_4$  phase coatings on  $\text{Al}_2\text{O}_3(0001)$  substrates has been employed, involving magnetron sputtering at room temperature on a designed composite target consisting of an underlying CrB target overlapped with a variable number of Al slices, followed by *ex situ* post-annealing in Ar for crystallization. The Cr:B ratio of the coatings has maintained close to 1 regardless of the varying Al content. The loss of Al during high-temperature annealing necessitates precise control over the Al content and the annealing temperature to ensure the production of phase-pure  $\text{Cr}_2\text{AlB}_2$  and  $\text{Cr}_4\text{AlB}_4$  coatings. Specifically, as-deposited coatings with a Cr:Al:B ratio close to the stoichiometry of  $\text{Cr}_2\text{AlB}_2$  are recommended to be annealed at the temperature range of 650–800 °C for dense, phase-pure and well-crystallized  $\text{Cr}_2\text{AlB}_2$  coatings. In contrast, obtaining well-crystallized  $\text{Cr}_4\text{AlB}_4$  coatings has proved challenging, possibly due to the loss of Al at high crystallization temperatures (over 700 °C) required for this phase. Our findings substantiate the rationality of the topotactic formation mechanism of  $\text{Cr}_2\text{AlB}_2$  and  $\text{Cr}_4\text{AlB}_4$  phases, wherein Al intercalates into CrB nuclei to drive the transformation from amorphous phases to crystalline Cr-Al-B MAB phases. Importantly, this transformation process did not yield CrB or Al phases, which could be attributed to the atomic-level mixing of atoms.

The innovative design of our composite target affords flexible control over the Al content of the coatings while ensuring the homogeneous mixing of elements sourced from discrete CrB and Al bulks. It is worth emphasizing that the parallel configuration of target-substrates plays a pivotal role in maintaining the Cr:B ratio of the coatings close to 1, which is not typically available in general combinatorial sputtering using tilt-fixed targets. Our approach to fabricating phase-pure and dense  $\text{Cr}_2\text{AlB}_2$  coatings holds promise for application in other MAB phases.

**Supplementary Materials:** The following supporting information can be downloaded at: <https://www.mdpi.com/article/10.3390/coatings13101800/s1>, Figure S1: Combinatorial sputtering of CrB and Al targets; Figure S2: GIXRD patterns measured on the post-annealed coatings deposited at sites (a), (b), and (c).

**Author Contributions:** Conceptualization, Z.L., G.W. and K.J.; methodology, K.J., G.W., Y.L. and S.D.; validation, K.J.; formal analysis, K.J.; investigation, K.J., Y.L. and S.D.; resources, Z.L., G.W. and S.L.; data curation, K.J.; writing—original draft preparation, K.J.; writing—review and editing, Z.L. and G.W.; visualization, K.J.; supervision, Z.L. and G.W.; project administration, Z.L.; funding acquisition, Z.L. and G.W. All authors have read and agreed to the published version of the manuscript.

**Funding:** This research was funded by the National Natural Science Foundation of China (Grant No. 12375270) and the State Key Laboratory of New Ceramics and Fine Processing Tsinghua University (No. KF202118).

**Institutional Review Board Statement:** Not applicable.

**Informed Consent Statement:** Not applicable.

**Data Availability Statement:** Not applicable.

**Acknowledgments:** The authors would like to thank Dongyue CHEN and Jie GAO of Tsinghua University for their comments and help with the revision of the manuscript.

**Conflicts of Interest:** The authors declare no conflict of interest.

## References

1. Kota, S.; Sokol, M.; Barsoum, M.W. A progress report on the MAB phases: Atomically laminated, ternary transition metal borides. *Int. Mater. Rev.* **2019**, *65*, 226–255. [[CrossRef](#)]
2. Barsoum, M.W. The  $M_{N+1}AX_N$  phases: A new class of solids; Thermodynamically stable nanolaminates. *Prog. Solid State Chem.* **2000**, *28*, 201–281. [[CrossRef](#)]
3. Radovic, M.; Barsoum, M.W. MAX phases: Bridging the gap between metals and ceramics. *Am. Ceram. Soc. Bull.* **2013**, *92*, 20–27.
4. Lu, J.; Kota, S.; Barsoum, M.W.; Hultman, L. Atomic structure and lattice defects in nanolaminated ternary transition metal borides. *Mater. Res. Lett.* **2016**, *5*, 235–241. [[CrossRef](#)]
5. Ade, M.; Hillebrecht, H. Ternary Borides  $Cr_2AlB_2$ ,  $Cr_3AlB_4$ , and  $Cr_4AlB_6$ : The First Members of the Series  $(CrB_2)_nCrAl$  with  $n = 1, 2, 3$  and a Unifying Concept for Ternary Borides as MAB-Phases. *Inorg. Chem.* **2015**, *54*, 6122–6135. [[CrossRef](#)] [[PubMed](#)]
6. Kota, S.; Wang, W.; Lu, J.; Natu, V.; Opagiste, C.; Ying, G.; Hultman, L.; May, S.J.; Barsoum, M.W. Magnetic properties of  $Cr_2AlB_2$ ,  $Cr_3AlB_4$ , and CrB powders. *J. Alloys Compd.* **2018**, *767*, 474–482. [[CrossRef](#)]
7. Sokol, M.; Natu, V.; Kota, S.; Barsoum, M.W. On the Chemical Diversity of the MAX Phases. *Trends Chem.* **2019**, *1*, 210–223. [[CrossRef](#)]
8. Jeitschko, W. Die Kristallstruktur von MoAlB. *Monatsh. Chem.* **1966**, *97*, 1472–1476. [[CrossRef](#)]
9. Li, N.; Bai, Y.; Wang, S.; Zheng, Y.; Kong, F.; Qi, X.; Wang, R.; He, X.; Duff, A.I. Rapid synthesis, electrical, and mechanical properties of polycrystalline  $Fe_2AlB_2$  bulk from elemental powders. *J. Am. Ceram. Soc.* **2017**, *100*, 4407–4411. [[CrossRef](#)]
10. Zhang, H.; Dai, F.-z.; Xiang, H.; Zhang, Z.; Zhou, Y. Crystal structure of  $Cr_4AlB_4$ : A new MAB phase compound discovered in Cr-Al-B system. *J. Mater. Sci. Technol.* **2019**, *35*, 530–534. [[CrossRef](#)]
11. Qi, X.; He, X.; Yin, W.; Song, G.; Zheng, Y.; Bai, Y. Stability trend, weak bonding, and magnetic properties of the Al- and Si-containing ternary-layered borides MAB phases. *J. Am. Ceram. Soc.* **2022**, *106*, 1513–1530. [[CrossRef](#)]
12. Gonzalez-Julian, J. Processing of MAX phases: From synthesis to applications. *J. Am. Ceram. Soc.* **2020**, *104*, 659–690. [[CrossRef](#)]
13. Kota, S.; Zapata-Solvas, E.; Ly, A.; Lu, J.; Elkassabany, O.; Huon, A.; Lee, W.E.; Hultman, L.; May, S.J.; Barsoum, M.W. Synthesis and Characterization of an Alumina Forming Nanolaminated Boride: MoAlB. *Sci. Rep.* **2016**, *6*, 26475. [[CrossRef](#)]
14. Kota, S.; Chen, Y.; Wang, J.; May, S.J.; Radovic, M.; Barsoum, M.W. Synthesis and characterization of the atomic laminate  $Mn_2AlB_2$ . *J. Eur. Ceram. Soc.* **2018**, *38*, 5333–5340. [[CrossRef](#)]
15. Zou, M.; Bao, L.; Yang, A.; Duan, Y.; Peng, M.; Cao, Y.; Li, M. Structural, elastic, mechanical, electronic, damage tolerance, fracture toughness, and optical properties of Cr-Al-B MAB phases studied by first-principles calculations. *J. Mater. Res.* **2023**, *38*, 1396–1409. [[CrossRef](#)]
16. Zhang, H.; Kim, J.Y.; Su, R.; Richardson, P.; Xi, J.; Kisi, E.; O'Connor, J.; Shi, L.; Szlufarska, I. Defect behavior and radiation tolerance of MAB phases ( $MoAlB$  and  $Fe_2AlB_2$ ) with comparison to MAX phases. *Acta Mater.* **2020**, *196*, 505–515. [[CrossRef](#)]
17. Zhang, D.; Richardson, P.; Tu, H.; O'Connor, J.; Kisi, E.; Zhang, H.; Shi, L. Radiation damage of MoAlB at elevated temperatures: Investigating MAB phases as potential neutron shielding materials. *J. Eur. Ceram. Soc.* **2022**, *42*, 1311–1321. [[CrossRef](#)]
18. Kim, J.Y.; Zhang, H.; Su, R.; Xi, J.; Wei, S.; Richardson, P.; Liu, L.; Kisi, E.; Perepezko, J.H.; Szlufarska, I. Defect recovery processes in Cr-B binary and Cr-Al-B MAB phases: Structure-dependent radiation tolerance. *Acta Mater.* **2022**, *235*, 118099. [[CrossRef](#)]
19. Li, C.; Tu, H.; Zhang, D.; Zhu, D.; Shi, L. Deuterium erosion and retention properties on MoAlB ceramics by ion irradiation. *Vacuum* **2023**, *207*, 111691. [[CrossRef](#)]
20. Zhang, H.; Xiang, H.; Dai, F.-Z.; Zhang, Z.; Zhou, Y. Oxidation behavior and thermal stability of  $Cr_2AlB_2$  powders. *Corros. Sci.* **2020**, *176*, 108941. [[CrossRef](#)]
21. Zhang, H.; Dai, F.-Z.; Xiang, H.; Wang, X.; Zhang, Z.; Zhou, Y. Phase pure and well crystalline  $Cr_2AlB_2$ : A key precursor for two-dimensional CrB. *J. Mater. Sci. Technol.* **2019**, *35*, 1593–1600. [[CrossRef](#)]
22. Dai, F.-Z.; Zhang, H.; Xiang, H.; Zhou, Y. Theoretical investigation on the stability, mechanical and thermal properties of the newly discovered MAB phase  $Cr_4AlB_4$ . *J. Mater. Sci. Technol.* **2020**, *39*, 161–166. [[CrossRef](#)]
23. Hanner, L.A.; Kota, S.; Barsoum, M.W. Formation mechanisms of  $Cr_2AlB_2$ ,  $Cr_3AlB_4$ , and  $Fe_2AlB_2$  MAB phases. *Mater. Res. Lett.* **2021**, *9*, 323–328. [[CrossRef](#)]
24. Berastegui, P.; Riekehr, L.; Jansson, U. Magnetron Sputtering of Nanolaminated  $Cr_2AlB_2$ . *Coatings* **2020**, *10*, 735. [[CrossRef](#)]
25. Zhang, Y.; Zhang, G.; Wang, T.; Wang, C.; Xie, Z.; Wang, W.; Xin, T. Synthesis, microstructure and properties of MoAlB MAB phase films. *Ceram. Int.* **2023**, *49*, 23714–23720. [[CrossRef](#)]
26. Tang, C.; Klimenkov, M.; Jaentsch, U.; Leiste, H.; Rinke, M.; Ulrich, S.; Steinbrück, M.; Seifert, H.J.; Stueber, M. Synthesis and characterization of  $Ti_2AlC$  coatings by magnetron sputtering from three elemental targets and ex-situ annealing. *Surf. Coat. Technol.* **2017**, *309*, 445–455. [[CrossRef](#)]
27. Kanatzidis, M.G.; Pöttgen, R.; Jeitschko, W. The Metal Flux: A Preparative Tool for the Exploration of Intermetallic Compounds. *Angew. Chem. Int. Ed.* **2005**, *44*, 6996–7023. [[CrossRef](#)] [[PubMed](#)]
28. Achenbach, J.-O.; Sahu, R.; Völker, B.; Hans, M.; Primetzhofner, D.; Miljanovic, D.J.; Scheu, C.; Schneider, J.M. Synthesis and Properties of Orthorhombic MoAlB Coatings. *Coatings* **2019**, *9*, 510. [[CrossRef](#)]

**Disclaimer/Publisher's Note:** The statements, opinions and data contained in all publications are solely those of the individual author(s) and contributor(s) and not of MDPI and/or the editor(s). MDPI and/or the editor(s) disclaim responsibility for any injury to people or property resulting from any ideas, methods, instructions or products referred to in the content.